AMERICAN SOCIETY FOR MICROBIOLOGY | Infection and Immunity®

BACTERIAL INFECTIONS

Burkholderia pseudomallei as an Enteric Pathogen: Identification of Virulence Factors Mediating Gastrointestinal Infection

Javier I. Sanchez-Villamil,[a] Daniel Tapia,[a] Grace I. Borlee,[c] Bradley R. Borlee,[c] David H. Walker,[b] Alfredo G. Torres[a,b]

[a]Department of Microbiology and Immunology, University of Texas Medical Branch, Galveston, Texas, USA
[b]Department of Pathology, University of Texas Medical Branch, Galveston, Texas, USA
[c]Department of Microbiology, Immunology, and Pathology, Colorado State University, Fort Collins, Colorado, USA

Javier I. Sanchez-Villamil and Daniel Tapia contributed equally to this article. Author order was determined alphabetically.

ABSTRACT *Burkholderia pseudomallei* is a Gram-negative bacterium and the causative agent of melioidosis. Despite advances in our understanding of the disease, *B. pseudomallei* poses a significant health risk, especially in regions of endemicity, where treatment requires prolonged antibiotic therapy. Even though the respiratory and percutaneous routes are well documented and considered the main ways to acquire the pathogen, the gastrointestinal tract is believed to be an underreported and underrecognized route of infection. In the present study, we describe the development of *in vitro* and *in vivo* models to study *B. pseudomallei* gastrointestinal infection. Further, we report that the type 6 secretion system (T6SS) and type 1 fimbriae are important virulence factors required for gastrointestinal infection. Using a human intestinal epithelial cell line and mouse primary intestinal epithelial cells (IECs), we demonstrated that *B. pseudomallei* adheres, invades, and forms multinucleated giant cells, ultimately leading to cell toxicity. We demonstrated that mannose-sensitive type 1 fimbria is involved in the initial adherence of *B. pseudomallei* to IECs, although the impact on full virulence was limited. Finally, we also showed that *B. pseudomallei* requires a functional T6SS for full virulence, bacterial dissemination, and lethality in mice infected by the intragastric route. Overall, we showed that *B. pseudomallei* is an enteric pathogen and that type 1 fimbria is important for *B. pseudomallei* intestinal adherence, and we identify a new role for T6SS as a key virulence factor in gastrointestinal infection. These studies highlight the importance of gastrointestinal melioidosis as an understudied route of infection and open a new avenue for the pathogenesis of *B. pseudomallei*.

KEYWORDS *Burkholderia pseudomallei*, melioidosis, GI infection, virulence factors

Melioidosis is a life-threatening disease with a wide range of complications caused by the Gram-negative saprophytic bacterium *Burkholderia pseudomallei* (1). The current geographic endemicity of *B. pseudomallei* includes Southeast Asia and northern Australia, but recent studies have expanded this distribution to be worldwide, including regions of the tropics (1, 2). Human melioidosis is associated with a high mortality rate, which can reach up to 40% in regions of endemicity, and several reports suggest the disease to be underreported throughout the world (1, 2). Current estimates propose that the global disease burden is approximately 165,000 new cases each year, of which ~89,000 are fatal (2). The intrinsic ability of *B. pseudomallei* to survive in diverse soil conditions of regions of endemicity has led to the prediction that its geographical distribution includes several countries and tropical regions (3, 4).

Citation Sanchez-Villamil JI, Tapia D, Borlee GI, Borlee BR, Walker DH, Torres AG. 2021. *Burkholderia pseudomallei* as an enteric pathogen: identification of virulence factors mediating gastrointestinal infection. Infect Immun 89:e00654-20. https://doi.org/10.1128/IAI.00654-20.

Editor Andreas J. Bäumler, University of California, Davis

Address correspondence to Alfredo G. Torres, altorres@utmb.edu.

Received 15 October 2020
Accepted 15 October 2020
Accepted manuscript posted online 26 October 2020
Published 15 December 2020

Melioidosis can develop after subcutaneous infection, ingestion, or inhalation of contaminated particles or aerosols. Although the percutaneous and inhalational routes of infection are well documented, the intragastric route of inoculation is underrecognized and understudied (1, 5). Reports of intragastric infection, though scarce, have been reported. In a recent study conducted in northeast Thailand, *B. pseudomallei* was isolated from 9/83 (11%) of stool samples and 9/58 (16%) rectal swabs from 141 patients with melioidosis (6). In a Malaysian study of patients with suspected *Helicobacter pylori* infection, of 215 gastric biopsy specimens, 15 (7%) contained *B. pseudomallei* cultures, of which 10 cases were also culture positive for *H. pylori*, and 5 contained only *B. pseudomallei* (7). Nonetheless, it is not known whether people with melioidosis develop persistent gut colonization and are capable of long-term shedding of *B. pseudomallei* in the stool (7). However, it is very likely that individuals that live in areas of endemicity can acquire the organism by the consumption of contaminated food or water.

Despite the predicted global distribution of *B. pseudomallei* and the potential to acquire melioidosis by the consumption of contaminated products, only two previous reports have tried to elucidate the pathogenesis of *B. pseudomallei* in the gastrointestinal (GI) tract. The first study suggested that esophageal delivery of *B. pseudomallei* to C57BL/6 and BALB/c mice did not result in susceptibility to infection, with a 50% lethal dose (LD_{50}) greater than 7×10^8 CFU (8). Further, a later study reported the lethal dose of *B. pseudomallei* when delivered orally to BALB/c and C57BL/6 mice to be 1.04×10^7 and 7.1×10^6 CFU, respectively (9). These reports suggest that infection with *B. pseudomallei* by the oral route, though feasible, requires high bacterial doses to cause disease; however, it is evident that further studies are needed to understand the pathogenesis of *B. pseudomallei* in the GI tract.

Initial adherence to the intestinal mucosa is often one of the critical steps in establishing an infection for most enteric pathogens (10). Nonetheless, studies evaluating virulence factors involved in the adherence of *B. pseudomallei* to intestinal epithelial cells have not been described. Type IV pili have been shown to be important in *B. pseudomallei* adherence to lung epithelial cells and contribute to *in vivo* virulence (10). However, one of the most important mediators of enteric pathogen adherence to the intestinal mucosa is the type 1 fimbria (11). Type 1 fimbriae binds D-mannosylated sugar residues linked to cell receptors on the surface of the epithelium, helping with the establishment of a colonization niche and, in some cases, facilitating internalization (12).

Successful colonization and adherence to the epithelial surface is a required mechanism of invading bacteria to compete with the host microbiota and/or antagonize host defenses. Some Gram-negative bacteria utilize the type 6 secretion system (T6SS) to inject a myriad of effectors into host cells or competing bacteria, allowing the pathogen to thrive in a wide range of environments (13). The T6SS is a syringe-like structure that resembles a bacteriophage tail injection device. The tail of the needle is structurally composed of polymerized hemolysin coregulated (Hcp) proteins, while the cap end of the needle is composed of VgrG family proteins (14). *B. pseudomallei* codes for six genomic clusters of T6SS genes, also termed T6SS-1 through T6SS-6 (15, 16). Upon entry into the host and escape from the vacuole, *B. pseudomallei* utilizes the T6SS-1 for its intercellular dissemination in eukaryotic cells, including the induction of multinucleated giant cells (MNGCs) and, eventually, cell death (15, 16). To mediate various host cellular effects, the T6SS apparatus injects putative effectors with a wide range of functions into the host cell. For example, the VgrG2a of *Pseudomonas aeruginosa* is a protein that directly interacts with γ-tubulin ring complex (γ-TuRC), while VgrG1 protein from *Vibrio cholerae* and *Aeromonas hydrophila* contains an actin cross-linking protein, allowing for the rearrangement of the host cytoskeleton (17, 18). The C-terminal domain of the VgrG-5 of *B. pseudomallei* is required for MNGC formation and virulence in mice (19). However, no functional effectors have been associated with the pathogenesis of *B. pseudomallei* in the GI tract.

Therefore, the objective of this study was to first evaluate the ability of *B. pseu-*

domallei to adhere, invade, and survive within intestinal epithelial cells *in vitro*, to establish an *in vivo* model of gastrointestinal melioidosis, and to study the function of putative virulence factors during *B. pseudomallei* GI infection. Together, our results highlight the importance of the intragastric route as a portal of entry for *B. pseudomallei* infections and warrants the recognition of *B. pseudomallei* as a true enteric pathogen.

RESULTS

***B. pseudomallei* requires type 1 fimbria to adhere to IECs.** A key event early in the pathogenesis of most gastrointestinal pathogens is the adherence to the intestinal mucosa. It is well-known that many enteric pathogens use fimbrial appendages to start the colonization in the intestine (20). Further, intracellular pathogens utilize complex virulence systems for successful intracellular survival and intercellular movement, such as the T6SS (13). To test whether *B. pseudomallei* utilizes a functional fimbria to mediate adherence to intestinal epithelial cells (IECs), we evaluated several *B. pseudomallei* mutants with transposon insertions in two biosynthetic clusters encoding type 1 fimbria-associated proteins (Tn::2047 and Tn::2048) or, in the type 1 fimbriae major subunit, FimA (Tn::2049 and Tn::2050). At least three transposon mutants showed reduced adherence to hIECs, but only a single strain with an interruption of the *fimA* gene (Tn::2049) was associated with a statistically significant difference in adherence compared to *B. pseudomallei* WT (strain 1026b) (Fig. S1A and B in the supplemental material). To further test the functionality of FimA, we created an isogenic mutant (*B. pseudomallei* Δ*fimA*) in the parent *B. pseudomallei* WT strain K96243 and analyzed the role of FimA in plaque formation. In addition, to examine the role of the T6SS in mediating intercellular spread, a critical step in bacterial intracellular survival, an isogenic mutant in *hcp1* (*B. pseudomallei* Δ*hcp1*), a gene that encodes a critical component of the T6SS injectosome was constructed and used to evaluate the formation of plaques. Although complementation of each of these mutations would be ideal to restore the phenotypes, a potential gain-of-function experiment in a select agent is not permitted. A characteristic cytotoxic effect at late stages of infection is cell detachment, which can be visualized and quantified by the formation of plaques on cell monolayers. After 24 h of infection, we observed a decrease in plaque formation efficiency, although not a complete elimination was observed, like in the case of the T6SS as visualized by the formation of plaques in Giemsa-stained monolayers (Fig. 1A). However, we noticed a significant decrease in plaque formation efficiency in the absence of FimA (Fig. 1B). Next, we evaluated the role of FimA in adherence to human IECs (hIECs) and primary mouse IECs (mIECs). In the absence of FimA, we noticed a significant reduction in *B. pseudomallei* adherence in both human and mouse IECs compared to *B. pseudomallei* wild-type (WT) or *B. pseudomallei* Δ*hcp1* infections (Fig. 1C). To corroborate the involvement of type I fimbriae, a well-known mannose-sensitive adhesin, we pretreated hIEC or mIECs with D-mannose and confirmed that addition of this carbohydrate caused a reduction in the adherence of *B. pseudomallei* WT and *B. pseudomallei* Δ*hcp1* to levels comparable to the *B. pseudomallei* Δ*fimA* mutant (Fig. 1C). The adherence of *B. pseudomallei* to IECs was visualized and corroborated by the quantitative results. Using fluorescence microscopy, we observed fewer bacteria adhered to the surface of IECs in the absence of FimA than to *B. pseudomallei* WT or *B. pseudomallei* Δ*hcp1* (Fig. 1D) after 1 h postinfection. To further analyze the effect of FimA in a T6SS mutant background, we evaluated the adherence of the double mutant *B. pseudomallei* Δ*hcp1* Δ*fimA* on IECs and observed an equivalent reduction as *B. pseudomallei* Δ*fimA* (Fig. 1D). These results confirmed the functionality of type 1 fimbriae in the adherence of *B. pseudomallei* to IECs and suggested a role for fimbriae in the adherence of this intracellular pathogen to the intestinal mucosa. Interestingly, the complete ablation of plaques by *B. pseudomallei* Δ*hcp1*, in the absence of reduced adherence onto IECs, warranted further investigation.

***B. pseudomallei* stimulates the formation of multinucleated giant cells and plaques on intestinal epithelial cells, a phenotype that requires a functional T6SS.** The ability of *B. pseudomallei* to infect epithelial cells is a well-recognized and principal

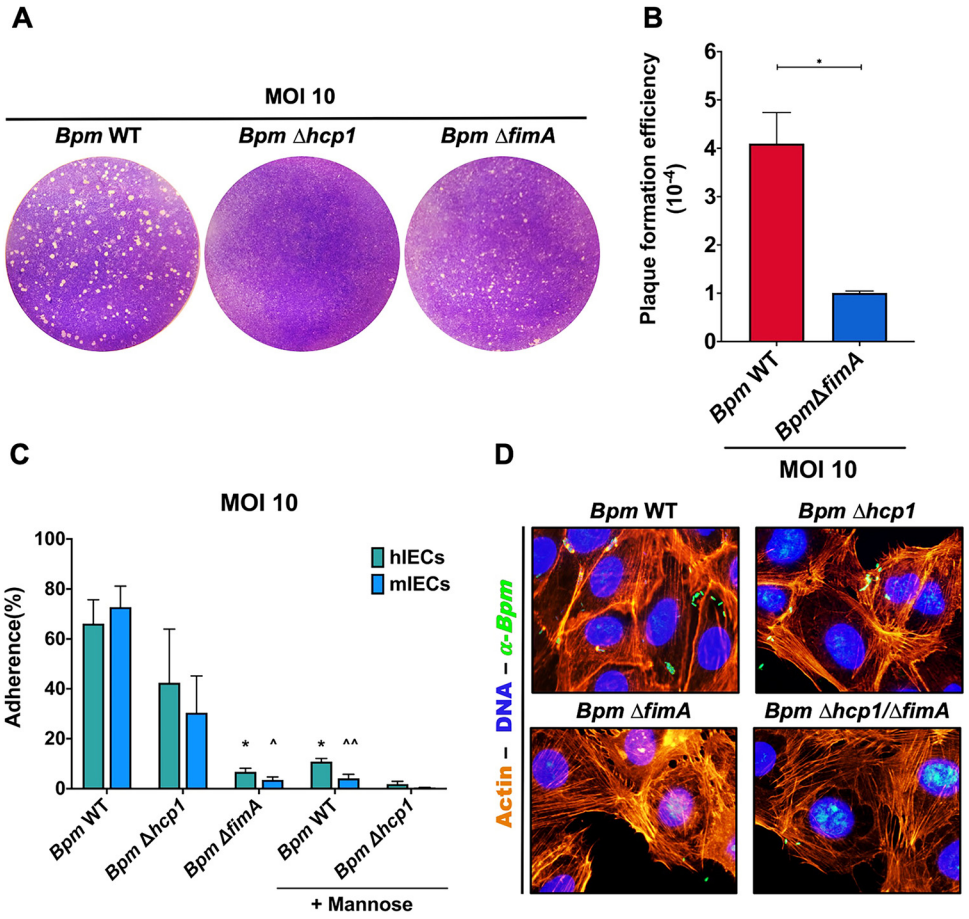

FIG 1 Type 1 fimbriae, a mannose-sensitive adhesin is involved in the adherence of *B. pseudomallei* (*Bpm*) to IECs. (A and B) Caco-2 cells were infected with *B. pseudomallei* WT, *B. pseudomallei* Δ*hcp1*, or *B. pseudomallei* Δ*fimA* for 24 h using an MOI of 10, washed, fixed, and then stained with Giemsa to visualize the formation of plaques. Plaque-forming efficiency was calculated as described in Materials and Methods. (C) Adhered bacteria to human or mouse IECs were quantified by CFU enumeration after 1 h. Prior to infection, IECs were incubated for 1 h in the presence or absence of 1% of D-mannose. *, $P < 0.05$ (comparison between hIECs). ^, $P < 0.05$, and ^^, $P < 0.01$ (comparison between mIECs). (D) Fluorescence microscopy of adhered *B. pseudomallei* WT, *B. pseudomallei* Δ*fimA*, *B. pseudomallei* Δ*hcp1*, or *B. pseudomallei* Δ*hcp1* Δ*fimA* on IECs for 1 h was visualized after staining for *B. pseudomallei*, actin, or DAPI. Error bars of the mean represent the average ± standard error of the mean of at least three experiments with three biological replicates. Statistical analysis was done using a Student's *t* test. Statistical differences between adherences were calculated by a two-way analysis of variance (ANOVA) followed by Tukey's *post hoc* test. *, $P < 0.05$.

route for bacterial entry (1). However, despite previous reports showing the ability of *B. pseudomallei* to cause lethality in mice infected intragastrically, no reports on the establishment of relevant models to study the biology or mechanisms of intestinal infection have been undertaken. Upon internalization, *B. pseudomallei* is able to move intercellularly by fusing host cells together and subsequently disseminating to distal organs, including the liver and spleen (1). To study the potential of *B. pseudomallei* to invade intestinal epithelial cells, we infected and subsequently visualized internalized bacteria in human-derived Caco-2 intestinal epithelial cells (hIECs) 24 h after infection (Fig. 2A). *B. pseudomallei* induced the formation of MNGCs by disruption of cellular membranes, leading to the formation of syncytia and the condensation of nuclei (Fig. 2A, center). In the absence of a functional T6SS, *B. pseudomallei* was unable to induce the condensation of cell nuclei or the formation of MNGCs in hIECs, and rather, *B. pseudomallei* remained confined to the intracellular cytoplasmic space (Fig. 2A, right). To visualize plaque formation, we infected hIECs or mIECs and quantified the efficiency of plaque formation 24 h after infection (Fig. 2B and C). The infection with *B. pseudomallei* WT resulted in the formation of plaques in monolayers of hIECs and

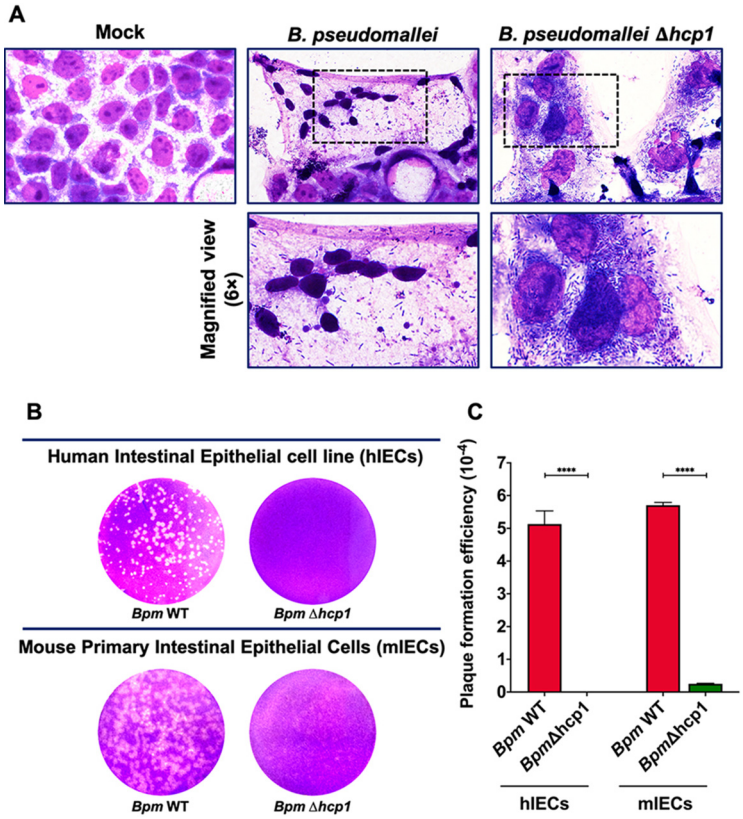

FIG 2 The formation of MNGCs and plaques in monolayers of intestinal epithelial cells requires a functional *B. pseudomallei* T6SS. (A) Human Caco-2 and mouse (C57BL/6) primary small intestine epithelial cells were infected with *B. pseudomallei* K96243 (WT) or *B. pseudomallei* Δ*hcp1* mutant for 24 h at 37°C and 5% CO_2, using an MOI of 10. After infection, cells were washed and stained with Giemsa and examined. (B) Giemsa-stained plaques were visualized by bright field microscopy (×60 magnification). Magnified view from the dotted-outlined area (×6) shows MNGC and cell nuclei contraction in *B. pseudomallei* WT infection but not in a *B. pseudomallei* T6SS mutant. (C) Plaque formation efficiency was calculated as described in Materials and Methods. Error bars represent the average ± standard error of the mean of at least three experiments with three biological replicates. Statistical analysis was done using a two-way ANOVA followed by a Tukeýs *post hoc* test. ****, $P < 0.0001$.

mIECs (Fig. 2B) with equivalent efficiency in mediating this effect. In the absence of a functional T6SS, this phenotype is reduced in hIECs and, to a lesser extent, in mIECs (Fig. 2B and C). The mIECs were validated by the phenotypic expression of cytokeratin-18 and ZO-1, two important markers of epithelial cells (Fig. S2A). Together, these results showed the ability of *B. pseudomallei* to infect human and mouse IECs, leading to the formation of syncytia, plaques, and subsequent cell death, an *in vitro* phenotype dependent on a functional T6SS.

***B. pseudomallei* can move from cell to cell and stimulate formation of MNGCs on IECs, a mechanism dependent on the T6SS.** To understand the intracellular lifestyle of *B. pseudomallei* as a gastrointestinal pathogen, we evaluated the ability of the bacteria to spread from cell to cell in hIECs and primary mIECs. Actin filaments and nuclei were stained using rhodamine-phalloidin and 4′,6-diamidino-2-phenylindole (DAPI), respectively, and bacterial cells were visualized using an antibody recognizing *Burkholderia* lipopolysaccharide (LPS). Starting at 12 h of infection, *B. pseudomallei* disrupted the cell cytoskeleton forming unipolar actin tails, allowing for intercellular movement (Fig. 3A and B). By 24 h after infection, this effect led to the formation of MNGCs (cell membranes denoted by dotted line) indicating fusion of cells; these effects were more pronounced in primary mIECs (Fig. 3B, arrows). To test the functionality of the T6SS on bacterial movement and the subsequent formation of MNGCs, we assessed the time course of infection using a T6SS-deficient strain. In the absence of the

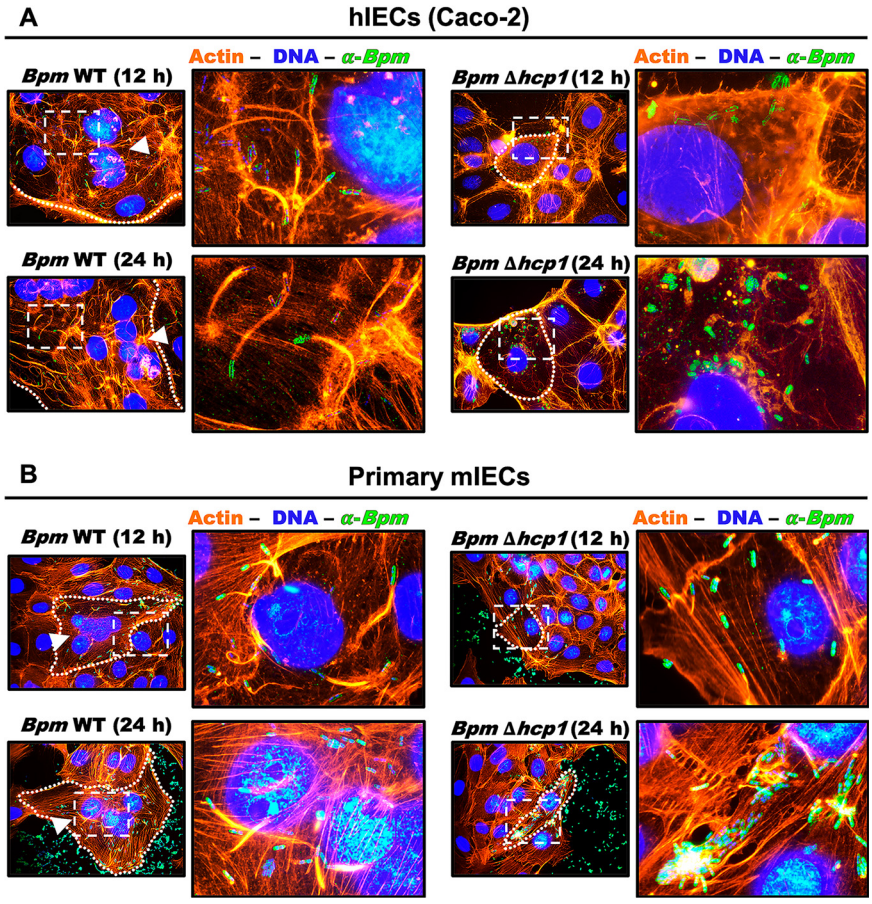

FIG 3 *B. pseudomallei* (*Bpm*) spreads intercellularly and causes formation of MNGC in IECs using a functional T6SS. Caco-2 (A) and mouse intestinal epithelial cells (mIECs) (B) were infected with *B. pseudomallei* WT or *B. pseudomallei* Δ*hcp1* for 12 and 24 h at 37°C and 5% CO_2, using an MOI of 10. After infection, cells were washed with PBS, fixed, and stained for immunofluorescence prior to microscopic examination (×60). Bacterial cells were stained with mouse anti-*Burkholderia* LPS polyclonal antibody, followed by an Alexa fluorophore 488 goat anti-mouse IgG secondary antibody. Actin was stained using rhodamine-phalloidin and cell nuclei with DAPI. Magnified view (×10) of dotted-outlined area is shown on the right side of each panel. Arrowheads indicate the presence of MNGC in *B. pseudomallei* WT-infected IECs. Images were processed and analyzed using ImageJ analysis software.

T6SS, the formation of MNGCs due to membrane fusion was not observed, and, in comparison to the *B. pseudomallei* WT infection, the integrity of the cell membrane in the monolayer remained intact (Fig. 3A and B). *B. pseudomallei* Δ*hcp1* remained trapped in the cytoplasm of individual cells, while the formation of actin tails was not affected (Fig. 3A and B, right panels). However, we observed a reduction in actin tail formation efficiency and length in both hIECs and mIECs in the absence of a functional T6SS (Fig. 3A and B and Fig. S2C). This effect may be due to a potential cross-communication mechanism between the T6SS and the BimA autotransporter, which is the protein associated with the induction of actin tails. These data further confirm that *B. pseudomallei* causes fusion of IECs, allowing the formation of MNGCs, an effect not seen in a T6SS-deficient strain, while the capacity of *B. pseudomallei* to form actin tails and move within the cell was minimally impacted.

***B. pseudomallei* is efficient in IEC intracellular replication and induction of cell death, mechanisms involving a functional T6SS, but not in IEC internalization.** To quantitatively assess the internalization of *B. pseudomallei* and the involvement of the T6SS in intracellular survival, we measured the internalization and fold change of intracellular replication within IECs. The internalization efficiency of *B. pseudomallei* WT and *B. pseudomallei* Δ*hcp1* at 3 h postinfection is equivalent for both strains, with

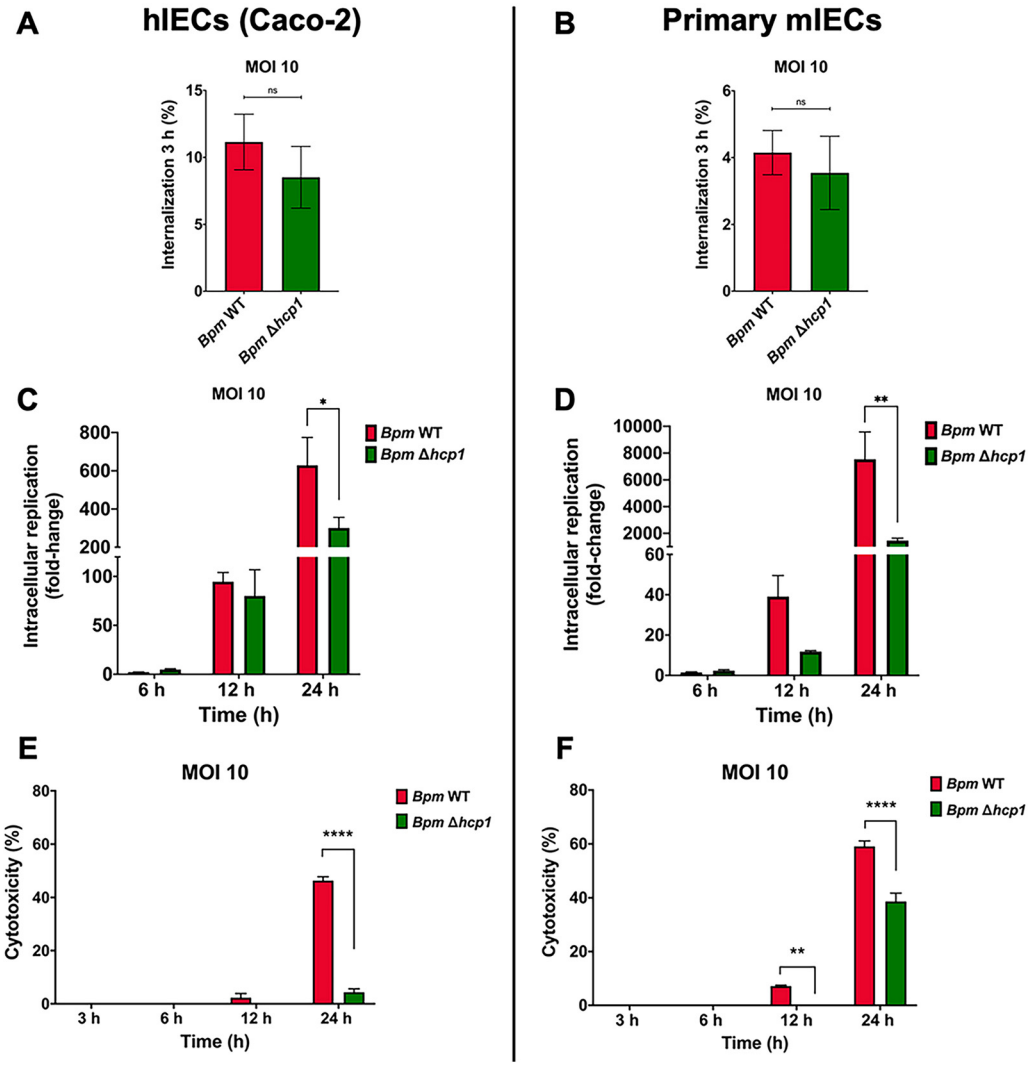

FIG 4 *B. pseudomallei* (*Bpm*) is highly efficient in IEC intracellular replication and in the induction of cytotoxicity, effects partially dependent on a functional T6SS, but not IEC internalization. (A and B) Percentage of internalized bacteria after 3 h postinfection. IECs were infected as described in Materials and Methods, and after 3 h, cells were washed and lysed. (C and D) Intracellular bacterial replication was quantified by CFU enumeration, and the fold change of intracellular replication was calculated from internalized bacteria 3 h postinfection. (E and F) Cell supernatants were collected after each time point and centrifuged, and LDH release was measured. The percentage of cell cytotoxicity was calculated following the manufacturer's instructions. Error bars of the mean represent the average ± standard error of the mean of at least three experiments with three biological replicates. Statistical analysis was done using a two-way ANOVA followed by a Tukeý́s *post hoc* test. Internalization statistical difference at 3 h postinfection was calculated by Student's *t* test. *, $P < 0.05$; **, $P < 0.01$; ****, $P < 0.0001$.

approximately 10% and 4% for hIECs and mIECs, respectively (Fig. 4A and B). Using hIECs and primary mIECs, we measured the fold change in intracellular replication after 6, 12, and 24 h of infection compared to an early time point of infection (3 h postinfection). Infection of hIECs with *B. pseudomallei* WT resulted in an increase of 100 times of intracellular replication at 12 h and a larger increment of approximately 600 times by 24 h, compared to 3 h postinfection (Fig. 4C). A similar pattern of intracellular replication was observed using primary mIECs, although in this case, *B. pseudomallei* was more efficient, with approximately 7,000-fold change in intracellular replication by 24 h compared with 3 h postinfection (Fig. 4D). In the absence of a functional T6SS, the relative fold change of intracellular replication was significantly lower by 24 h in both hIECs and mIECs (Fig. 4C and D). Based on our previous observation showing the formation of plaques and the disruption of cell membrane integrity, we assessed the

ability of *B. pseudomallei* to induce cell cytotoxicity by measuring the release of lactate dehydrogenase (LDH), indicative of the disruption of cell membrane integrity and a release of intracellular LDH (21). Cell culture supernatants were taken after each infection time point, and these results showed that IECs infected with *B. pseudomallei* WT exhibited a higher percentage of cytotoxicity beginning with 12 h after infection and a more pronounced effect at 24 h postinfection (Fig. 4E and F). Cells infected with *B. pseudomallei* Δ*hcp1* showed a significant reduction in cytotoxicity of approximately 10% at 12 h after infection and a reduction of approximately 40% and 20% by 24 h in hIECs and primary mIECs, respectively (Fig. 4E and F). Compared to hIECs, primary mIECs appear to have a higher susceptibility to infection with *B. pseudomallei* Δ*hcp1* (Fig. 4E and F). Together, these results indicate that at 24 h postinfection, *B. pseudomallei* WT is able to replicate more efficiently than *B. pseudomallei* Δ*hcp1*, an effect likely due to the ability of bacteria to induce cell death and multiplication in the extracellular milieu. Also, these results demonstrate the internalization efficiency of *B. pseudomallei* in IECs and indicate the dependence of a functional T6SS to cause cell toxicity.

***B. pseudomallei* can infect and disseminate in acute and chronic mouse models of infection.** Given the remarkable ability of *B. pseudomallei* to adhere and invade mIECs and induce cell cytotoxicity, we used a mouse model to assess the virulence of *B. pseudomallei* when delivered by the intragastric route. The LD_{50} of *B. pseudomallei* K96243 was calculated based on the Reed and Muench method and determined to be 1 $LD_{50} = 2.5 \times 10^6$ CFU per mouse (22). To assess the virulence of *B. pseudomallei* after GI infection in an acute murine model, we infected animals with 2.5 LD_{50} equivalents ($\sim 6.25 \times 10^6$ CFU/mouse) of *B. pseudomallei* WT via gavage and evaluated survival for 21 days (Fig. 5A). Three days after infection, animals infected with *B. pseudomallei* WT showed 30% survival, with only 3/10 animals surviving to the endpoint of the experiment (Fig. 5B). To assess the role of either the type 1 fimbriae or the T6SS during infection, we inoculated animals with 2.5 LD_{50} equivalents of *B. pseudomallei* Δ*hcp1*, *B. pseudomallei* Δ*fimA*, or *B. pseudomallei* Δ*hcp1* Δ*fimA*, and assessed survival for up to days 21 postinfection. Among animals that were inoculated with *B. pseudomallei* Δ*hcp1* or *B. pseudomallei* Δ*hcp1* Δ*fimA*, the lethality was reduced at 21 days postinfection, with a significant difference in percent survival compared to *B. pseudomallei* WT (Fig. 5B). In contrast, the *B. pseudomallei* Δ*fimA* mutant displayed a similar lethality rate as the *B. pseudomallei* WT. We collected fecal samples for 3 days after infection and were not able to recover any shed bacteria (limit of detection of 10). To further determine whether *B. pseudomallei* can colonize the GI tract, we collected segments of the GI tract (stomach plus small intestine or cecum plus colon) of surviving animals to quantify bacterial loads (Fig. 5C). Animals infected with *B. pseudomallei* WT that survived to the endpoint of the experiment had no recoverable bacteria in any of the organs evaluated, with a limit of detection of 1 CFU (Fig. 5C). This suggests that surviving animals infected with *B. pseudomallei* WT had resolved the infection. However, animals that were inoculated with *B. pseudomallei* Δ*hcp1*, *B. pseudomallei* Δ*fimA*, or *B. pseudomallei* Δ*hcp1* Δ*fimA* carried at the 21-day endpoint, approximately 10^1 to 10^2 CFU/g of tissue in the colon and small intestine, respectively (Fig. 5C).

Given the lethality of *B. pseudomallei* in our acute model of infection and the role of T6SS in the *in vivo* pathogenic process, we assessed whether *B. pseudomallei* disseminates to distal organs using a chronic melioidosis infection model (Fig. 5A). Animals were inoculated with a sublethal dose ($\sim$1 LD_{50}) of either *B. pseudomallei* WT, *B. pseudomallei* Δ*hcp1*, *B. pseudomallei* Δ*fimA*, or *B. pseudomallei* Δ*hcp1* Δ*fimA*, and survival was assessed for 35 days (Fig. 5A). Animals that were inoculated with *B. pseudomallei* WT exhibited 40% (4/10) survival at 35 days postinfection (dpi), while 90% of animals that were inoculated with *B. pseudomallei* Δ*hcp1* or *B. pseudomallei* Δ*fimA*, and 100% (10/10) receiving *B. pseudomallei* Δ*hcp1* Δ*fimA*, survived to the end of the study (Fig. 5D). Bacterial load was evaluated by collecting individual sections of the GI tract (stomach, small intestine, cecum, and colon), as well as the liver and spleen of surviving animals, which were processed for CFU enumeration (Fig. 5E). Animals inoculated with *B. pseudomallei* WT exhibited persistent colonization of the stomach, small intestine,

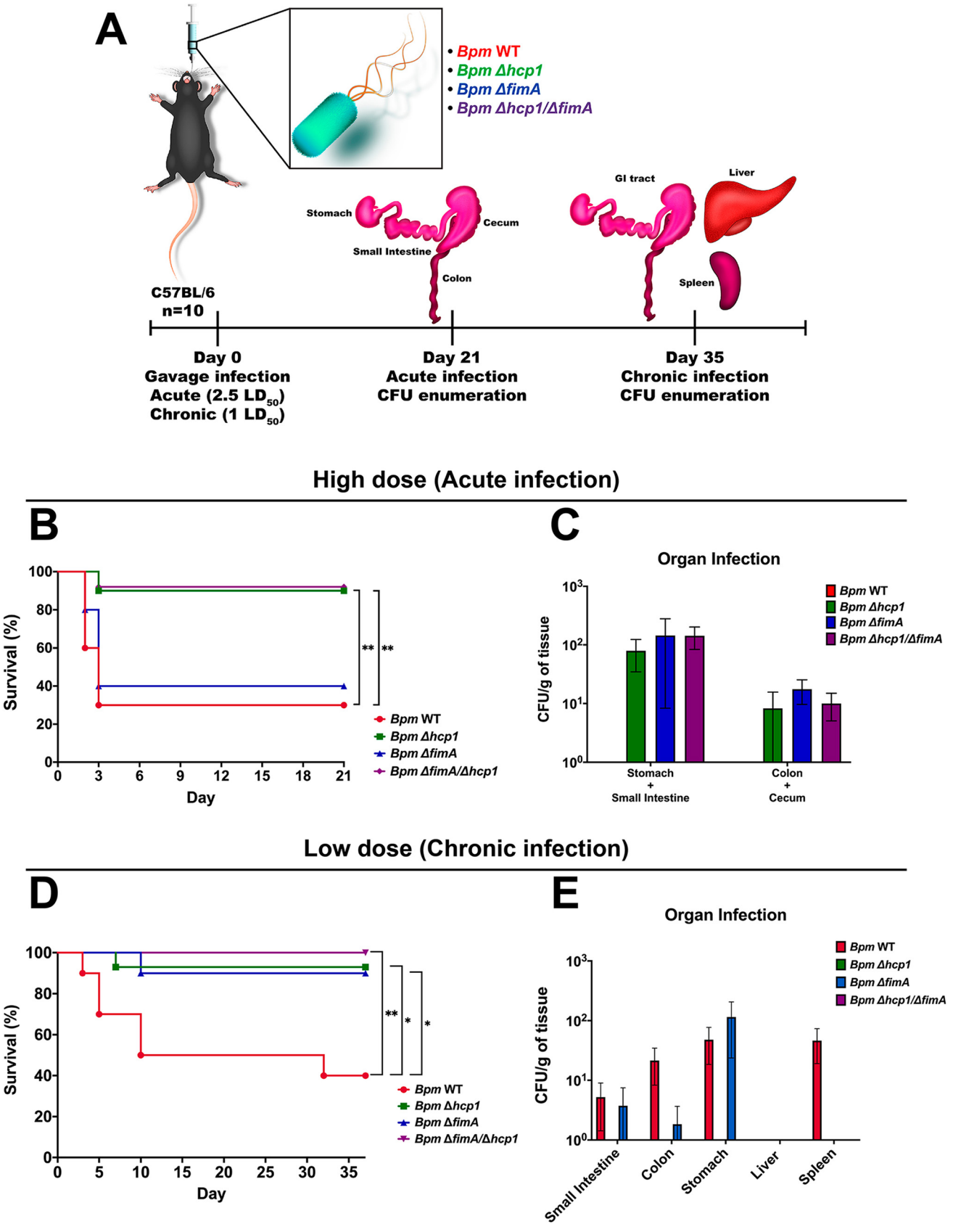

FIG 5 Functional virulence factors are required for pathogenesis of *B. pseudomallei* (*Bpm*) in acute and chronic gastrointestinal mouse models of melioidosis infection. (A) Timeline of gastrointestinal infection. Animals ($n = 10$) were infected via gavage with a low (acute)- or high (chronic)-dose equivalents of 2.5

(Continued on next page)

and colon, with the largest CFU numbers in the stomach ($\sim 10^2$ CFU/gram of tissue) (Fig. 5E). In the case of the single and double *B. pseudomallei* mutants, only the *B. pseudomallei* Δ*fimA* strain persisted and colonized the stomach, small intestine, and colon. No bacteria were recovered in the liver of any infected group, and only the *B. pseudomallei* WT-infected animals developed dissemination to the spleen (Fig. 5E). Overall, our data demonstrate the ability of *B. pseudomallei* to colonize the stomach and the intestine with subsequent dissemination to the spleen, a virulence phenotype mainly dependent on GI-expressed virulence factors.

DISCUSSION

Melioidosis infections are associated with a high mortality rate (1), and acquisition of the pathogen occurs through different routes of infection, including percutaneous inoculation, and inhalation, and more recently, oral ingestion has been reported in clinical cases (6). A previous report of *B. pseudomallei* infection by the intragastric route suggested the stomach as the primary site of *B. pseudomallei* gastrointestinal colonization, although no mechanistic studies were performed to understand the pathogenesis of *B. pseudomallei* following oral inoculation (9). These observations are consistent with our results showing the stomach with the highest level of *B. pseudomallei* colonization after oral inoculation.

The *B. pseudomallei* T6SS forms an injectosome that has been associated with different mechanisms of interbacterial competition as well as the delivery of mediators involved in host-pathogen interactions. The T6SS-1 of *Burkholderia thailandensis* and *B. pseudomallei* has been demonstrated to be involved in the formation of MNGCs and plaque formation in different *in vitro* cell models (15, 16). To study GI infection and the contribution of different virulence factors to infection, we optimized a model to study *B. pseudomallei* pathogenesis, allowing us to evaluate bacterial adhesion, invasion, and dissemination. Our results demonstrate that *B. pseudomallei* efficiently induces these hallmarks of pathogenesis in a type 1 fimbria- and T6SS-dependent manner. MNGCs are a result of cellular membrane fusion by mechanisms not entirely understood by either mechanical forces involving bacterial motility or bacterial effectors involved in membrane fusion (23). The formation of MNGCs leads to cellular death and detachment (24). It is interesting to note the differences observed in bacterial infectivity between mIECs and hIECs. As such, mIECs appear to be more susceptible to *B. pseudomallei* Δ*hcp1* infection, indicating that other virulence factors not associated with the T6SS and additional factors expressed in murine primary cells may be partially involved in MNGC and plaque formation. We also observed the condensation of cellular nuclei, also known as pyknosis, indicative of the induction of cell death (23). In contrast, these effects were not observed in a T6SS-deficient strain. The results suggest the importance of other T6SS-associated factors in mediating these processes, as it occurs in the absence of VgrG, the only other *B. pseudomallei* T6SS factor which is unable to mediate membrane fusion during intercellular spread and MNGC formation (19, 25). Given that Hcp functions as a T6SS-associated effector protein (26, 27), exogenous addition of the Hcp1 protein was unable to restore *in vitro* MNGC formation or plaques (Fig. S3 in the supplemental material). These results confirm that an intact T6SS is required to translocate the effector protein(s) that are needed to mediate cell-to-cell spread and MNGC formation. By utilizing a human-derived Caco-2 cell line, we were able to recapitulate *in vitro* certain aspects of the pathogenesis of *B. pseudomallei*. However, due to the transformed nature of these cellular models, they are often unable to express and

FIG 5 Legend (Continued)
LD_{50} ($\sim 6.25 \times 10^6$ CFU/mouse) or 1 LD_{50} (2.5×10^6 CFU/mouse), respectively, of *B. pseudomallei* WT, *B. pseudomallei* Δ*hcp1*, *B. pseudomallei* Δ*fimA*, or *B. pseudomallei* Δ*hcp1* Δ*fimA*. The oral gavage LD_{50} of *B. pseudomallei* K96243 was calculated using the Reed and Muench method (22) and estimated to be $\sim 2.5 \times 10^6$ CFU per mouse. (B and D) Survival curves of animals infected with each strain in either the acute or chronic infection models. Twenty-one days (acute) or 35 days (chronic) after infection, the stomach, small intestine, colon, cecum, liver, and spleen were collected and processed to quantify bacterial load by CFU. (C and E) Bacterial colonization in the acute and chronic studies was determined by CFU per gram of tissue. Error bars of the mean represent the average ± standard error of the mean of at least three experiments with three biological replicates Statistical analysis was done using a log-rank test. *, $P < 0.05$; **, $P < 0.01$.

localize receptors or have disrupted intracellular signaling (28–30). Considering these limitations, we decided to test our findings in primary intestinal epithelial cells obtained from C57BL/6 mice (the same genetic background as the mice used during challenges). Because our findings appeared to recapitulate the natural pathogenesis process of *B. pseudomallei in vitro*, we recommend that future studies of *B. pseudomallei* in IECs should use primary cells as a more biologically relevant infection model.

Intracellular pathogens exploit the host cell actin cytoskeleton for intercellular movement within the cytoplasm (31). This mechanism is crucial for intracellular enteric pathogens such as *Salmonella*, *Listeria*, and *Shigella*, allowing for their dissemination upon entry (31). In order for an intracellular bacterium to hijack the host cytoskeleton, the T3SS plays an important role in the subversion of host processes and polarly localized proteins as initiators of actin-based motility (32). These hallmarks of pathogenesis were recapitulated in our study with both IECs, obtaining comparable results. In the absence of a functional T6SS, we were still able to see the formation of actin tails, though smaller in length in the primary mIECs, suggesting a potential difference in the efficiency of actin tail formation in these cells, but the underlying molecular mechanism is yet to be defined. Interestingly, the size differences in actin tail length in primary mIECs between *B. pseudomallei* WT and *B. pseudomallei* Δ*hcp1* is also suggestive of an association between the T6SS and the virulence factors which work in concert for efficient actin tail formation. This observation has also been reported for *Burkholderia mallei*, a closely related pathogen with a high degree of genetic identity to *B. pseudomallei* (33). Consistent with this prediction, we were also able to see the formation of actin tails, MNGCs, and plaques by *B. mallei* in mIECs (Fig. S1B). Despite the inability to disrupt the formation of actin tails in the absence of a T6SS, we did not observe membrane fusion or MNGC formation, leaving the bacteria trapped in the cytoplasm. These findings further support that a functional T6SS is essential to mediate membrane fusion and subsequent intercellular bacterial spreading in the host (34).

Given the effective way *B. pseudomallei* multiplies intracellularly and evade host defense mechanisms in both phagocytic and nonphagocytic cells (15), it is surprising that the bacterial mechanisms required to colonize and invade intestinal epithelial cells, as well as the disruption of the cell membrane barrier to promote dissemination, are not understood. We have shown that *B. pseudomallei* enters hIECs and primary mIECs, with a greater efficiency observed in mIECs. The intracellular replication of *B. pseudomallei* and the induction of a cytopathic effect in both IECs is dependent on a functional T6SS, suggesting that this mechanism is important for bacterial survival and dissemination to other cells and tissues. The induction of cell cytopathology by other enteric bacteria has been shown to be a strategy for subsequent dissemination and establishment of a new niche (35). The detection of LDH released from infected IECs is a key characteristic of necrotic cells and is linked to the permeabilization of the cell plasma membrane (36). As observed here, in the absence of the T6SS, *B. pseudomallei* remains confined within the cell cytoplasm, and it is associated with a reduced cytopathic effect, suggesting that other factors involved earlier in the pathogenesis, like BopE (37), may be involved in mediating this effect.

Many gastrointestinal pathogens exploit mannose residues on mucosal epithelial cells for internalization using a variety of adhesin molecules, including type 1 fimbriae (12, 38, 39). Our results showed that although we did not completely block plaque formation in the absence of type 1 fimbriae, a delay in adherence to IECs was observed compared to the *B. pseudomallei* WT. The reduction in adherence in the presence of exogenous mannose supports the notion that *B. pseudomallei* carries functional mannose-dependent type 1 fimbriae. Our cumulative *in vitro* studies demonstrate that we have identified two virulence factors involved in the pathogenic process of *B. pseudomallei* upon contact with intestinal epithelial cells. Although we have not performed complementation experiments because *B. pseudomallei* is a select agent and, therefore, a potential gain of function experiment is not permitted, our studies are opening the door for future studies to define the potential mechanism required for gastrointestinal melioidosis.

Different surrogate small animal models have been developed to study various aspects of melioidosis while using different routes of infection, including inhalational and subcutaneous inoculation (40, 41). However, few studies have focused on the establishment of *in vivo* models that recapitulate either the acute or chronic (sublethal) stages of infection by the GI route. A previous report showed that an intragastric mouse model of melioidosis infection, using BALB/c and C57BL/6 mice, required a high infection dose of 7×10^8 CFU/mouse for successful *B. pseudomallei* infection (8). In contrast, our studies demonstrate that the lethality of *B. pseudomallei* in the C57BL/6 mouse acute infection model was achieved with a lower dose and that bacterial dissemination to distal organs was observed using our sublethal model of infection. Another study in BALB/c mice using a sublethal dose (5×10^5 CFU) of *B. pseudomallei* led to the establishment of persistent intragastric infection and concluded that *B. pseudomallei* was infectious in both the acute and chronic murine models, an effect dependent on the challenge dose (9). However, it is important to highlight that differences in bacterial strains, mouse genotypes, or mouse microbiomes may account for some of the differences observed. Our studies were consistent with previous reports showing no to low levels of bacterial shedding in the stools of acutely infected animals, suggesting that *B. pseudomallei* may be efficiently and quickly internalized into IECs and bacteria do not remain in the intestinal lumen (8, 9). In addition, we have reported that *B. pseudomallei* colonizes the GI tract during chronic infection, with the largest bacterial load recovered from the stomach, an interesting finding that warrants further studies to understand the potential mechanism of bacterial entry or survival in a nonpermissive environment for bacterial colonization. Further, our results are consistent with clinical studies that have found *B. pseudomallei* in human gastric biopsy specimens (42, 43). However, it is important to emphasize the remarkable ability of *B. pseudomallei* to survive in the acidic environment of the stomach, which led us to speculate that *B. pseudomallei* might share some features found in *H. pylori*, which is capable of producing urease, an enzyme which catalyzes the hydrolysis of urea to yield ammonia, thus elevating the pH of its environment (44). Another interesting observation of our *in vivo* murine model was the inability of *B. pseudomallei* to infect the spleen in the absence of a functional T6SS, strengthening its functionality in mediating intercellular bacterial movement and dissemination from the intestine to distal organs.

Our results also showed that the absence of FimA does not have a strong effect on the lethality of the mutant strain compared to WT infection at high infection dose, which suggests that type 1 fimbriae are not a critical virulence factor during this *in vivo* condition. This observation could be due to a dose-response effect, whereby a higher number of bacteria might overcome the absence of type 1 fimbria. Further, our *in vitro* observations reflect the attenuation of *B. pseudomallei* Δ*fimA* in the low-dose infection model. In addition, these results could also suggest that *B. pseudomallei* has a wide repertoire of factors that promote efficient colonization and internalization during acute infection. However, the difference in survival in the chronic infection model between the *B. pseudomallei* Δ*fimA* and the *B. pseudomallei* WT suggests that FimA, in a low infectious dose, is required for full lethal infection, and its absence delays the establishment of effective colonization along the GI tract. This effect may be more translatable to human infections from the ingestion of low-dose *B. pseudomallei*-contaminated sources.

The use of our acute and chronic murine melioidosis models, together with the previous report (9), should be used to define additional virulence factors required for gastrointestinal colonization, information that could be useful to expand our understanding of human gastrointestinal melioidosis infection. Taken together, we were able to highlight the fact that *B. pseudomallei* uses specific virulence factors to cause gastrointestinal infection and warrant the classification of *B. pseudomallei* as an enteric pathogen. In addition, the establishment of both the *in vivo* and *in vitro* gastrointestinal models of *B. pseudomallei* infection opens the door to further studies in identifying additional virulence factors, such as those T6SS-injected effectors associated with intracellular survival, MNGC formation, cell death, and/or bacterial dissemination

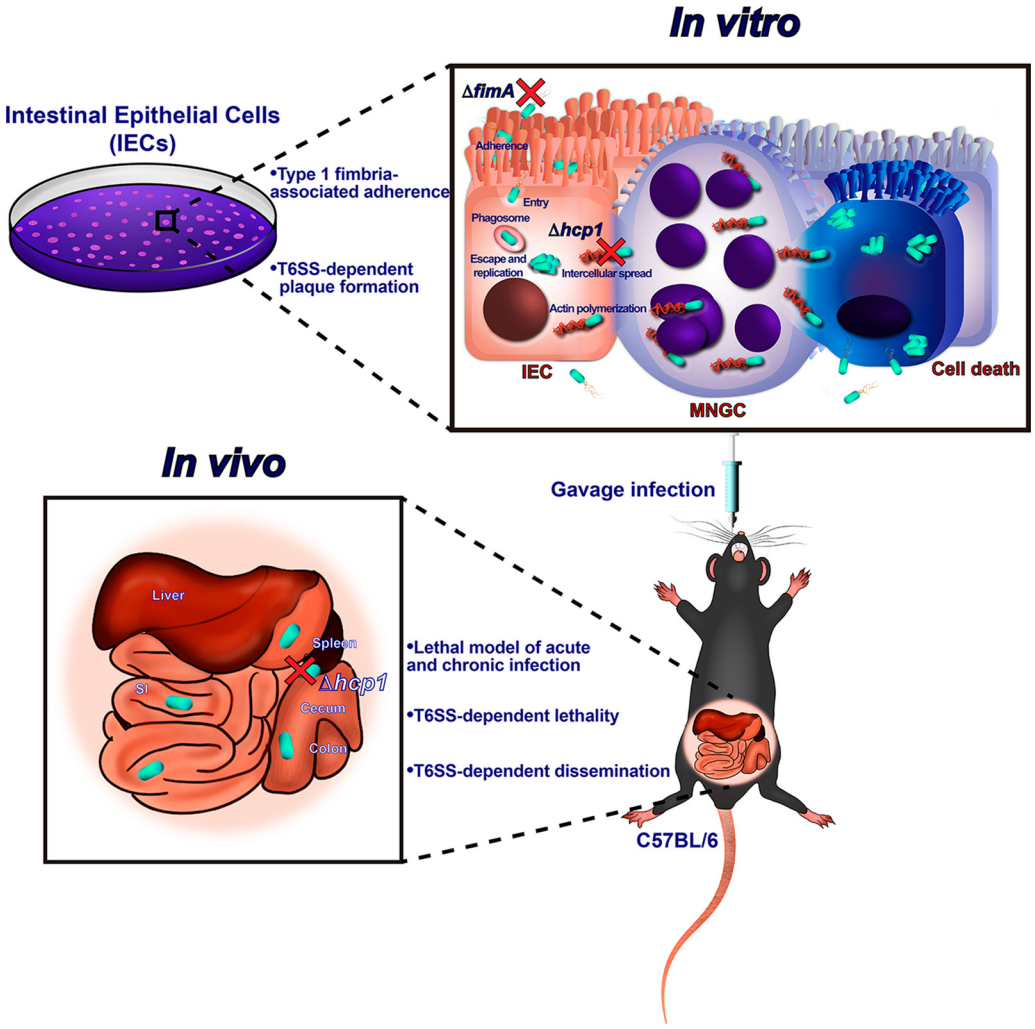

FIG 6 Graphical model of *B. pseudomallei* gastrointestinal infection. A model depicting the key findings of *B. pseudomallei* gastrointestinal pathogenesis, both *in vivo* and *in vitro*. MNGC, multinucleated giant cell; SI, small intestine; T6SS, type VI secretion system.

(Fig. 6). Finally, we have highlighted the importance of gastrointestinal melioidosis as an understudied route of infection.

MATERIALS AND METHODS

Bacterial strains and growth conditions. *B. pseudomallei* and *B. mallei* strains were routinely grown at 37°C in Luria-Bertani (LB) medium containing 1% NaCl, LB with 4% glycerol (LBG), or Ashdown's selection medium with gentamicin (Sigma-Aldrich) specific for *B. pseudomallei*.

Transposon mutants. The *B. pseudomallei* transposon insertion mutants in fimbriae biosynthetic genes used in this study were identified from a sequence-defined library of T24 transposon mutants in *B. pseudomallei* 1026b as previously described (45). All work with *B. pseudomallei* 1026b T24 mutants at Colorado State University was performed in a biosafety level 3 (BSL3) facility approved to work with tier 1 select agents. Transposon insertion mutants Tn::2047 (Bp1026b_I1572), Tn::2048 (Bp1026b_I1572), Tn::2049 (Bp1026b_I1759), and Tn::2050 (Bp1026b_I1759) were confirmed by PCR followed by sequencing. *B. pseudomallei* 1026b T24 mutants were maintained on media containing 300 μg/ml kanamycin (Gold Biotechnology, Saint Louis, MO).

Construction of mutants. All isogenic mutants, including the *B. pseudomallei* Δ*hcp1* (gene BPSS1498), *B. pseudomallei* Δ*fimA* (gene BPSL1629), and *B. pseudomallei* Δ*fimA* Δ*hcp1* strains were constructed using a select agent-compliant suicide vector allelic exchange system as previously described (46). For the single mutants, the 500 bp upstream and downstream of *hcp1* or *fimA* genes were cloned into plasmid pMo130 and introduced into the donor *Escherichia coli* S17-1 λ*pir* strain. Five hundred microliters of *E. coli* donor strain were mixed with 500 μl of *B. pseudomallei* K96243, centrifuged, and resuspended in 100 μl of 10 mM $MgSO_4$ as a mix or individual strains for controls. Each conjugation was spotted (25 μl) on LBG agar and incubated for 8 to 16 h at 37°C. Selection of merodiploids was

performed by resuspending the mixed reactions in Dulbecco's phosphate-buffered saline (DPBS), and the diluted solutions were plated on LBG agar containing 500 μg/ml of kanamycin to select for integration and 30 μg/ml of polymyxin B to select against the donor *E. coli* strain. The plates were incubated for 48 to 96 h at 37°C. Merodiploids were screened by exposing the plates to 0.45 M pyrocatechol solution for selection of yellow colonies that integrated the plasmid. Counterselection was performed by subculturing merodiploids in 2× yeast extract-tryptone (2×YT) broth without salt for 4 h and then plating on 2×YT agar without salt and supplemented with 15% sucrose for 48 to 72 h. The resulting colonies were then screened with pyrocatechol, and nonyellow colonies were screened by PCR to confirm the mutation of *hcp1* or *fimA*. Colonies positive by PCR were then sequenced to confirm the mutation. The double mutant strain, *B. pseudomallei* Δ*fimA* Δ*hcp1*, was constructed by using *B. pseudomallei* strain CLH010 (Δ*hcp1*) and introducing the *fimA* mutation using pMo130 plasmid as described previously (47, 48). The single Δ*hcp1* mutant was confirmed using primers described previously (48). The single and double Δ*fimA* mutations were then confirmed by PCR, followed by sequencing using the following primers: forward, 5′-CCG CCC TGC AGC GGA TCC CTC TAG ACA ACC GCT CGG CGA GAC C, and reverse, 5′-GAC AAG CCC GTC GCA TGC ATC TAG ACT GGC CGA GCA GCG TCA CGT TGA CCT GC.

Cell infection assays and immunofluorescence microscopy. The human colorectal adenocarcinoma cell line (Caco-2; ATCC HTB-37) or C57BL/6 mouse primary small intestinal epithelial cells (catalog no. C57-6051, Cell Biologics Inc., Chicago, IL) were routinely grown in Dulbecco's modified Eagle medium (DMEM) or complete primary cell culture medium following the manufacturer's instructions (catalog no. M6621, Cell Biologics Inc.). DMEM medium was supplemented with 0.1 mM nonessential amino acid, 100 U penicillin/ml, 100 μg of streptomycin/ml (Gibco), and 10% fetal bovine serum (FBS) (Gibco). Cells were incubated at 37°C and 5% CO_2. For microscopic analysis, 5×10^5 CFU were grown in 12-well cell-culture grade plates (Corning) or coverslips previously treated with type IV collagen from human placenta (BioReagent) and incubated overnight prior to treatment. Cells were infected with *B. pseudomallei* wild type (WT), *B. pseudomallei* Δ*hcp1*, *B. pseudomallei* Δ*fimA*, or *B. pseudomallei* Δ*hcp1* Δ*fimA* using a multiplicity of infection (MOI) of 10 for 1 h. After infection, cells were washed twice with PBS and fresh medium containing 1 mg/ml of kanamycin (Km) for an additional hour. For plaque formation analysis, upon extracellular bacterial killing for 1 h, a semisolid 0.25% agarose overlay containing 500 μg/ml of Km in the medium was added for 24 h. After infection, cells were fixed with 4% paraformaldehyde (PFA) in phosphate-buffered saline (PBS) for 30 min, stained with Giemsa stain (Gibco) for 30 min, and washed with PBS. For immunofluorescence microscopic analysis, infected human and mouse epithelial cells were fixed with 4% PFA and permeabilized with 0.1% Triton X-100 in PBS for 5 min prior to staining. Bacteria were detected with serum from lipopolysaccharide (LPS)-immunized mice (1:500), followed by a goat anti-mouse IgG, IgM (H+L) secondary antibody conjugated to Alexa 488. Polymerized actin and DNA were visualized using rhodamine isothiocyanate-phalloidin (Molecular Probes, Invitrogen, USA) or DAPI (Molecular Probes, Invitrogen), respectively. Cells were mounted using ProLong Gold antifade (Molecular Probes, Invitrogen) prior to visualization. Quantification of actin tail length was done by measuring the length of at least 200 tails from representative images at 24 h postinfection using the Olympus cellSens imaging software v2.3. Images were examined using an Olympus BX51 upright fluorescence microscope and analyzed using ImageJ software, National Institutes of Health (49).

Bacterial adherence, internalization, and intracellular replication assays. Human and mouse intestinal epithelial cells were grown to confluence (5×10^5) in a 12-well plate prior to infection as described above with some modifications. For adherence, prior to infection, bacteria were incubated in the presence or absence of 1% of D-mannose (Sigma) for 1 h at 37°C. Prior to infection, the inoculum was calculated based on optical density (OD) of the *B. pseudomallei* culture and plated to quantify the input inoculum. After 1 h of incubation, cells were infected with each strain for 1 h. After infection, cells were washed three times with PBS and lysed in the presence of 0.1% Triton X-100, and adhered bacteria were quantified by CFU enumeration. To measure the percentage of bacterial internalization, cells were infected for 1 h with each strain and then washed prior to replacing with fresh medium containing 1 mg/ml of Km for 1 h. After 3 h, internalized bacteria were quantified by CFU enumeration compared to the input inoculum. Fold change in intracellular replication was determined by CFU enumeration at 6, 12, and 24 h postinfection, in relation to 3 h postinfection after three washes with PBS and cell lysis with 0.1% Triton X-100. To assess cell cytotoxicity, supernatants were collected at each time point, spun at $5{,}000 \times g$ for 5 min, and immediately used to assay for lactate dehydrogenase (LDH) release. The percentage of internalized bacteria was quantified according to the equation internalized bacteria at 3 h/input inoculum × 100. The fold change in intracellular replication was quantified according to the equation surviving bacteria at each time point/internalized bacteria at 3 h postinfection.

Lactate dehydrogenase release assay. The supernatants of infected cells after each time point of infection were collected for quantification of LDH release following the manufacturer's protocol (Sigma-Aldrich, St. Louis, MO). The percent cytotoxicity was calculated using the following formula: % cytotoxicity = 100 × (corrected reading from test well − corrected reading from untreated well)/(corrected maximum LDH control − corrected reading from untreated well). The corrected readings indicate the read from a test well minus the reading from the media-only control.

Ethics statement. All manipulations of *B. pseudomallei* were conducted in CDC/USDA-approved and registered BSL3 facilities at the University of Texas Medical Branch (UTMB) and Colorado State University (CSU) in accordance with approved BSL3 standard operating practices. The animal studies at UTMB were carried out humanely in strict accordance with the recommendations in the Guide for the Care and Use of Laboratory Animals by the National Institutes of Health. The protocol (IACUC no. 0503014D) was approved by the Animal Care and Use Committee of UTMB.

Animal studies. Female 6-to-8-week-old C57BL/6 mice ($n = 10$) were purchased from Jackson Laboratory (Bar Harbor, ME, USA) and maintained in an animal biosafety level 3 (ABSL3) facility. Animals were housed in microisolator cages under pathogen-free conditions with food and water available *ad libitum* and maintained on a 12-h light cycle.

Acute (high-dose) and chronic (low-dose) infection models. Food was restricted 12 h before infection but was administered throughout the remainder of the study. For the acute model of infection, animals were infected with 2.5 LD_{50} equivalents of *B. pseudomallei* WT (K96243), *B. pseudomallei* Δ*hcp1*, *B. pseudomallei* Δ*fimA*, or *B. pseudomallei* Δ*hcp1* Δ*fimA* using a plastic oral gavage needle. Five fecal pellets were taken from each mouse every day, homogenized, centrifuged (5,000 × *g* for 5 min), plated on Ashdown *B. pseudomallei*-selective medium containing gentamicin, and incubated at 37°C. The LD_{50} of *B. pseudomallei* K96243 was determined using an in-house calculation (1 $LD_{50} = 2.5 \times 10^6$ CFU per mouse) calculated based on the Reed and Muench method (22). For the chronic infection model, mice ($n = 10$) were infected with ~1 LD_{50} equivalent as described above. At 21 or 35 days postinfection, mice were humanely euthanized, and the organs from surviving animals were collected and divided for determining bacterial loads. To enumerate bacterial loads, the gastrointestinal tract was divided into stomach and small intestine or cecum and colon in the acute model or all four separate compartments for the chronic model. Also, for the chronic study, the liver and spleen of surviving animals were collected. All organs were homogenized in 1 ml of PBS, serially diluted, and plated in either LB agar (spleen and liver) or Ashdown selective medium (GI tract) to quantify bacterial loads.

SUPPLEMENTAL MATERIAL

Supplemental material is available online only.

SUPPLEMENTAL FILE 1, PDF file, 0.4 MB.

ACKNOWLEDGMENTS

The manuscript was partially supported by NIH NIAID grant AI12660101 and UTMB seed funds awarded to A.G.T. D.T. was funded by an NIH NIAID Research Supplement for Underrepresented Minorities. J.I.S.-V. was supported by the Conacyt ConTex postdoctoral fellowship.

The contents are solely the responsibility of the authors and do not necessarily represent the official views of the NIAID or NIH.

J.I.S.-V. and D.T. designed the experiments; J.I.S.-V. and D.T. performed the experiments; G.I.B. identified and verified *B. pseudomallei* 1026b transposon mutants; and J.I.S.-V., D.T., G.I.B., B.R.B., D.H.W., and A.G.T. wrote the manuscript. J.I.S.-V., D.T., G.I.B., B.R.B., D.H.W., and A.G.T. edited and approved the manuscript.

REFERENCES

1. Wiersinga WJ, Virk HS, Torres AG, Currie BJ, Peacock SJ, Dance DAB, Limmathurotsakul D. 2018. Melioidosis. Nat Rev Dis Primers 4:17107. https://doi.org/10.1038/nrdp.2017.107.
2. Limmathurotsakul D, Golding N, Dance DA, Messina JP, Pigott DM, Moyes CL, Rolim DB, Bertherat E, Day NP, Peacock SJ, Hay SI. 2016. Predicted global distribution of *Burkholderia pseudomallei* and burden of melioidosis. Nat Microbiol 1:15008. https://doi.org/10.1038/nmicrobiol.2015.8.
3. Sanchez-Villamil JI, Torres AG. 2018. Melioidosis in Mexico, Central America, and the Caribbean. Trop Med Infect Dis 3:24. https://doi.org/10.3390/tropicalmed3010024.
4. Chewapreecha C, Holden MT, Vehkala M, Valimaki N, Yang Z, Harris SR, Mather AE, Tuanyok A, De Smet B, Le Hello S, Bizet C, Mayo M, Wuthiekanun V, Limmathurotsakul D, Phetsouvanh R, Spratt BG, Corander J, Keim P, Dougan G, Dance DA, Currie BJ, Parkhill J, Peacock SJ. 2017. Global and regional dissemination and evolution of *Burkholderia pseudomallei*. Nat Microbiol 2:16263. https://doi.org/10.1038/nmicrobiol.2016.263.
5. Wiersinga WJ, Currie BJ, Peacock SJ. 2012. Melioidosis. N Engl J Med 367:1035–1044. https://doi.org/10.1056/NEJMra1204699.
6. Teparrukkul P, Kongkasame W, Chitsaeng S, Wongsuwan G, Wuthiekanun V, Peacock SJ, Limmathurotsakul D. 2017. Gastrointestinal tract involvement in melioidosis. Trans R Soc Trop Med Hyg 111:185–187. https://doi.org/10.1093/trstmh/trx031.
7. Khosravi Y, Dieye Y, Poh BH, Ng CG, Loke MF, Goh KL, Vadivelu J. 2014. Culturable bacterial microbiota of the stomach of *Helicobacter pylori* positive and negative gastric disease patients. ScientificWorldJournal 2014:610421. https://doi.org/10.1155/2014/610421.
8. West TE, Myers ND, Limmathurotsakul D, Liggitt HD, Chantratita N, Peacock SJ, Skerrett SJ. 2010. Pathogenicity of high-dose enteral inoculation of *Burkholderia pseudomallei* to mice. Am J Trop Med Hyg 83:1066–1069. https://doi.org/10.4269/ajtmh.2010.10-0306.
9. Goodyear A, Bielefeldt-Ohmann H, Schweizer H, Dow S. 2012. Persistent gastric colonization with *Burkholderia pseudomallei* and dissemination from the gastrointestinal tract following mucosal inoculation of mice. PLoS One 7:e37324. https://doi.org/10.1371/journal.pone.0037324.
10. Essex-Lopresti AE, Boddey JA, Thomas R, Smith MP, Hartley MG, Atkins T, Brown NF, Tsang CH, Peak IR, Hill J, Beacham IR, Titball RW. 2005. A type IV pilin, PilA, contributes to adherence of *Burkholderia pseudomallei* and virulence *in vivo*. Infect Immun 73:1260–1264. https://doi.org/10.1128/IAI.73.2.1260-1264.2005.
11. Kolenda R, Ugorski M, Grzymajlo K. 2019. Everything you always wanted to know about *Salmonella* type 1 fimbriae, but were afraid to ask. Front Microbiol 10:1017. https://doi.org/10.3389/fmicb.2019.01017.
12. Avalos Vizcarra I, Hosseini V, Kollmannsberger P, Meier S, Weber SS, Arnoldini M, Ackermann M, Vogel V. 2016. How type 1 fimbriae help *Escherichia coli* to evade extracellular antibiotics. Sci Rep 6:18109. https://doi.org/10.1038/srep18109.
13. Hachani A, Wood TE, Filloux A. 2016. Type VI secretion and anti-host effectors. Curr Opin Microbiol 29:81–93. https://doi.org/10.1016/j.mib.2015.11.006.
14. Zoued A, Brunet YR, Durand E, Aschtgen MS, Logger L, Douzi B, Journet L, Cambillau C, Cascales E. 2014. Architecture and assembly of the type VI secretion system. Biochim Biophys Acta 1843:1664–1673. https://doi.org/10.1016/j.bbamcr.2014.03.018.
15. Lennings J, Makhlouf M, Olejnik P, Mayer C, Brotz-Oesterhelt H, Schwarz S. 2019. Environmental and cellular factors affecting the localization of

T6SS proteins in *Burkholderia thailandensis*. Int J Med Microbiol 309:151335. https://doi.org/10.1016/j.ijmm.2019.151335.
16. Lennings J, West TE, Schwarz S. 2018. The *Burkholderia* type VI secretion system 5: composition, regulation and role in virulence. Front Microbiol 9:3339. https://doi.org/10.3389/fmicb.2018.03339.
17. Durand E, Derrez E, Audoly G, Spinelli S, Ortiz-Lombardia M, Raoult D, Cascales E, Cambillau C. 2012. Crystal structure of the VgrG1 actin cross-linking domain of the *Vibrio cholerae* type VI secretion system. J Biol Chem 287:38190–38199. https://doi.org/10.1074/jbc.M112.390153.
18. Suarez G, Sierra JC, Erova TE, Sha J, Horneman AJ, Chopra AK. 2010. A type VI secretion system effector protein, VgrG1, from *Aeromonas hydrophila* that induces host cell toxicity by ADP ribosylation of actin. J Bacteriol 192:155–168. https://doi.org/10.1128/JB.01260-09.
19. Schwarz S, Singh P, Robertson JD, LeRoux M, Skerrett SJ, Goodlett DR, West TE, Mougous JD. 2014. VgrG-5 is a *Burkholderia* type VI secretion system-exported protein required for multinucleated giant cell formation and virulence. Infect Immun 82:1445–1452. https://doi.org/10.1128/IAI.01368-13.
20. Taylor RK. 1991. Bacterial adhesion to mucosal surfaces. J Chemother 3(Suppl 1):190–195.
21. Hou L, Liu K, Li Y, Ma S, Ji X, Liu L. 2016. Necrotic pyknosis is a morphologically and biochemically distinct event from apoptotic pyknosis. J Cell Sci 129:3084–3090. https://doi.org/10.1242/jcs.184374.
22. Reed LJ, Muench H. 1938. A simple method of estimating fifty per cent endpoints. Am J Epidemiol 27:493–497. https://doi.org/10.1093/oxfordjournals.aje.a118408.
23. Lim YT, Jobichen C, Wong J, Limmathurotsakul D, Li S, Chen Y, Raida M, Srinivasan N, MacAry PA, Sivaraman J, Gan YH. 2015. Extended loop region of Hcp1 is critical for the assembly and function of type VI secretion system in *Burkholderia pseudomallei*. Sci Rep 5:8235. https://doi.org/10.1038/srep08235.
24. French CT, Toesca IJ, Wu TH, Teslaa T, Beaty SM, Wong W, Liu M, Schroder I, Chiou PY, Teitell MA, Miller JF. 2011. Dissection of the *Burkholderia* intracellular life cycle using a photothermal nanoblade. Proc Natl Acad Sci U S A 108:12095–12100. https://doi.org/10.1073/pnas.1107183108.
25. Toesca IJ, French CT, Miller JF. 2014. The type VI secretion system spike protein VgrG5 mediates membrane fusion during intercellular spread by pseudomallei group *Burkholderia* species. Infect Immun 82:1436–1444. https://doi.org/10.1128/IAI.01367-13.
26. Mariano G, Trunk K, Williams DJ, Monlezun L, Strahl H, Pitt SJ, Coulthurst SJ. 2019. A family of type VI secretion system effector proteins that form ion-selective pores. Nat Commun 10:5484. https://doi.org/10.1038/s41467-019-13439-0.
27. Zhou Y, Tao J, Yu H, Ni J, Zeng L, Teng Q, Kim KS, Zhao GP, Guo X, Yao Y. 2012. Hcp family proteins secreted via the type VI secretion system coordinately regulate *Escherichia coli* K1 interaction with human brain microvascular endothelial cells. Infect Immun 80:1243–1251. https://doi.org/10.1128/IAI.05994-11.
28. Abreu MT. 2010. Toll-like receptor signalling in the intestinal epithelium: how bacterial recognition shapes intestinal function. Nat Rev Immunol 10:131–144. https://doi.org/10.1038/nri2707.
29. Elewaut D, DiDonato JA, Kim JM, Truong F, Eckmann L, Kagnoff MF. 1999. NF-kappa B is a central regulator of the intestinal epithelial cell innate immune response induced by infection with enteroinvasive bacteria. J Immunol 163:1457–1466.
30. Lacroix M. 2008. Persistent use of "false" cell lines. Int J Cancer 122:1–4. https://doi.org/10.1002/ijc.23233.
31. De Souza Santos M, Orth K. 2019. The role of the type III secretion system in the intracellular lifestyle of enteric pathogens. Microbiol Spectr 7. https://doi.org/10.1128/microbiolspec.BAI-0008-2019.
32. Vander Broek CW, Zainal Abidin N, Stevens JM. 2017. BipC, a predicted *Burkholderia pseudomallei* type 3 secretion system translocator protein with actin binding activity. Front Cell Infect Microbiol 7:333. https://doi.org/10.3389/fcimb.2017.00333.
33. Burtnick MN, DeShazer D, Nair V, Gherardini FC, Brett PJ. 2010. *Burkholderia mallei* cluster 1 type VI secretion mutants exhibit growth and actin polymerization defects in RAW 264.7 murine macrophages. Infect Immun 78:88–99. https://doi.org/10.1128/IAI.00985-09.
34. Chen Y, Wong J, Sun GW, Liu Y, Tan GY, Gan YH. 2011. Regulation of type VI secretion system during *Burkholderia pseudomallei* infection. Infect Immun 79:3064–3073. https://doi.org/10.1128/IAI.05148-11.
35. Flieger A, Frischknecht F, Hacker G, Hornef MW, Pradel G. 2018. Pathways of host cell exit by intracellular pathogens. Microb Cell 5:525–544. https://doi.org/10.15698/mic2018.12.659.
36. Chan FK, Moriwaki K, De Rosa MJ. 2013. Detection of necrosis by release of lactate dehydrogenase activity. Methods Mol Biol 979:65–70. https://doi.org/10.1007/978-1-62703-290-2_7.
37. Stevens MP, Friebel A, Taylor LA, Wood MW, Brown PJ, Hardt WD, Galyov EE. 2003. A *Burkholderia pseudomallei* type III secreted protein, BopE, facilitates bacterial invasion of epithelial cells and exhibits guanine nucleotide exchange factor activity. J Bacteriol 185:4992–4996. https://doi.org/10.1128/jb.185.16.4992-4996.2003.
38. Grzymajlo K, Ugorski M, Suchanski J, Kedzierska AE, Kolenda R, Jarzab A, Biernatowska A, Schierack P. 2017. The novel type 1 fimbriae FimH receptor calreticulin plays a role in *Salmonella* host specificity. Front Cell Infect Microbiol 7:326. https://doi.org/10.3389/fcimb.2017.00326.
39. Uchiya KI, Kamimura Y, Jusakon A, Nikai T. 2019. *Salmonella* fimbrial protein FimH Is involved in expression of proinflammatory cytokines in a toll-like receptor 4-dependent manner. Infect Immun 87:e00881-18. https://doi.org/10.1128/IAI.00881-18.
40. Warawa JM. 2010. Evaluation of surrogate animal models of melioidosis. Front Microbiol 1:141. https://doi.org/10.3389/fmicb.2010.00141.
41. Massey S, Yeager LA, Blumentritt CA, Vijayakumar S, Sbrana E, Peterson JW, Brasel T, LeDuc JW, Endsley JJ, Torres AG. 2014. Comparative *Burkholderia pseudomallei* natural history virulence studies using an aerosol murine model of infection. Sci Rep 4:4305. https://doi.org/10.1038/srep04305.
42. Currie BJ, Fisher DA, Howard DM, Burrow JN, Lo D, Selva-Nayagam S, Anstey NM, Huffam SE, Snelling PL, Marks PJ, Stephens DP, Lum GD, Jacups SP, Krause VL. 2000. Endemic melioidosis in tropical northern Australia: a 10-year prospective study and review of the literature. Clin Infect Dis 31:981–986. https://doi.org/10.1086/318116.
43. Puthucheary SD, Lin HP, Yap PK. 1981. Acute septicaemic melioidosis: a report of seven cases. Trop Geogr Med 33:19–22.
44. Celli JP, Turner BS, Afdhal NH, Keates S, Ghiran I, Kelly CP, Ewoldt RH, McKinley GH, So P, Erramilli S, Bansil R. 2009. *Helicobacter pylori* moves through mucus by reducing mucin viscoelasticity. Proc Natl Acad Sci U S A 106:14321–14326. https://doi.org/10.1073/pnas.0903438106.
45. Borlee GI, Plumley BA, Martin KH, Somprasong N, Mangalea MR, Islam MN, Burtnick MN, Brett PJ, Steinmetz I, AuCoin DP, Belisle JT, Crick DC, Schweizer HP, Borlee BR. 2017. Genome-scale analysis of the genes that contribute to *Burkholderia pseudomallei* biofilm formation identifies a crucial exopolysaccharide biosynthesis gene cluster. PLoS Negl Trop Dis 11:e0005689. https://doi.org/10.1371/journal.pntd.0005689.
46. Hamad MA, Zajdowicz SL, Holmes RK, Voskuil MI. 2009. An allelic exchange system for compliant genetic manipulation of the select agents *Burkholderia pseudomallei* and *Burkholderia mallei*. Gene 430:123–131. https://doi.org/10.1016/j.gene.2008.10.011.
47. Khakhum N, Bharaj P, Myers JN, Tapia D, Walker DH, Endsley JJ, Torres AG. 2019. Evaluation of *Burkholderia mallei* Δ*tonB* Δ*hcp1* (CLH001) as a live attenuated vaccine in murine models of glanders and melioidosis. PLoS Negl Trop Dis 13:e0007578. https://doi.org/10.1371/journal.pntd.0007578.
48. Mott TM, Vijayakumar S, Sbrana E, Endsley JJ, Torres AG. 2015. Characterization of the *Burkholderia mallei tonB* mutant and its potential as a backbone strain for vaccine development. PLoS Negl Trop Dis 9:e0003863. https://doi.org/10.1371/journal.pntd.0003863.
49. Schindelin J, Arganda-Carreras I, Frise E, Kaynig V, Longair M, Pietzsch T, Preibisch S, Rueden C, Saalfeld S, Schmid B, Tinevez JY, White DJ, Hartenstein V, Eliceiri K, Tomancak P, Cardona A. 2012. Fiji: an open-source platform for biological-image analysis. Nat Methods 9:676–682. https://doi.org/10.1038/nmeth.2019.